

ARL-TN-58

AR-008-404

**AD-A274 842**  
■■■■■■■■■■



**DTIC**  
ELECTE  
JAN 25 1994  
S C

**DEPARTMENT OF DEFENCE**  
**DEFENCE SCIENCE AND TECHNOLOGY ORGANISATION**  
**AERONAUTICAL RESEARCH LABORATORY**  
**MELBOURNE, VICTORIA**

Technical Note 58

**STRESS ANALYSIS OF A SECONDARY-BENDING SPECIMEN**

by

**R.L. EVANS**  
**M. HELLER**

Approved for public release

© COMMONWEALTH OF AUSTRALIA 1993

NOVEMBER 1993

**94-T-24-014**

**94-02036**  
■■■■■■■■■■

**This work is copyright. Apart from any use as permitted under the Copyright Act 1968, no part may be reproduced by any process without prior written permission from the Australian Government Publishing Services. Requests and enquiries concerning reproduction and rights should be addressed to the Manager, Commonwealth Information Services, Australian Government Publishing Services, GPO Box 84, Canberra ACT 2601.**

**THE UNITED STATES NATIONAL  
TECHNICAL INFORMATION SERVICE  
IS AUTHORISED TO  
REPRODUCE AND SELL THIS REPORT**

# DISCLAIMER NOTICE



THIS DOCUMENT IS BEST QUALITY AVAILABLE. THE COPY FURNISHED TO DTIC CONTAINED A SIGNIFICANT NUMBER OF COLOR PAGES WHICH DO NOT REPRODUCE LEGIBLY ON BLACK AND WHITE MICROFICHE.

AR-008-404

**DEPARTMENT OF DEFENCE  
DEFENCE SCIENCE AND TECHNOLOGY ORGANISATION  
AERONAUTICAL RESEARCH LABORATORY**

Technical Note 58

**STRESS ANALYSIS OF A SECONDARY-BENDING SPECIMEN**

by

**R.L. EVANS  
M. HELLER**

**SUMMARY**

*This Note describes a two-dimensional finite-element elastic analysis of a uniaxially-loaded bolted secondary-bending specimen which was conducted to provide information relevant to a recent ARL fatigue testing program. Three different approaches were employed to model the bolt/plate interface and the results are compared with thermoelastic stress measurements.*

**DTIC QUALITY INSPECTED 5**



© COMMONWEALTH OF AUSTRALIA 1993

**POSTAL ADDRESS:** Director, Aeronautical Research Laboratory  
506 Lorimer Street, Fishermens Bend  
Victoria 3207, Australia.

Accession For	
NTIS	CRA&I <input checked="" type="checkbox"/>
DTIC	TAB <input type="checkbox"/>
Unannounced <input type="checkbox"/>	
Justification:	
By	
Distribution /	
Availability Codes	
Dist	Avail and/or Special
A-1	

# CONTENTS

	Page
1. INTRODUCTION	1
2. SPECIMEN DETAILS	1
3. NUMERICAL ANALYSIS	1
3.1 Model 1	2
3.2 Model 2	2
3.3 Model 3	2
4. EXPERIMENTAL ANALYSIS	3
5. RESULTS AND DISCUSSION	3
5.1 Numerical Analysis	3
5.2 Experimental Analysis	4
5.3 Comparison of Experimental and Numerical Analyses	4
5.4 Comparison of U.K. and Numerical Data	5
6. CONCLUSIONS	6
REFERENCES	6
FIGURES 1 - 9	
APPENDIX A PAFEC data file for Model 1	
B PAFEC data file for Model 3	
C Secondary-bending ratio data	
DISTRIBUTION	
DOCUMENT CONTROL DATA	

## 1. INTRODUCTION

A test program has recently been undertaken at ARL to investigate the effect of secondary bending on the fatigue life of joints with and without hole cold-working and interference-fit bolts [1]. Secondary bending is caused by an eccentricity of the applied load relative to the neutral axis of a structural component, and results in the superposition of bending stresses on axial stresses. This Note describes a preliminary two-dimensional finite-element elastic analysis of a uniaxially-loaded bolted secondary-bending specimen which was conducted to provide information relevant to the ARL fatigue testing program. Thermoelastic tests were conducted, and the experimental results are compared with the finite-element-model analysis. Experimental information from the United Kingdom on similar specimens is also examined.

## 2. SPECIMEN DETAILS

The secondary-bending specimen analysed in this paper is depicted in Figure 1, and is a slightly modified version of the U.K. Q-joint [2]. It is composed of three main members (two 5 mm thick components, and one 3 mm thick component) fastened together with four bolts of 6.30 mm diameter. A 2 mm and a 5 mm spacer complete the specimen. (The modification with respect to the U.K. Q-joint is an extension of the gripping portion of the specimen from 60 mm to 75 mm to allow easier gripping in ARL test machines). The material is a high strength/weight aluminium alloy, namely 7075-T651, commonly used in the F/A-18 fighter aircraft, with the elastic properties  $E = 71$  GPa and  $\nu = 0.33$ .

## 3. NUMERICAL ANALYSIS

A total of eight models of differing degrees of rigidity were analysed. The three discussed in this report cover the range that were analysed and vary from a totally rigid joint to a much more flexible and realistic joint. The models are two-dimensional, assuming plane stress, while the actual specimen is of course three-dimensional, pertinently in the region of the bolts. On comparing Figure 1 of the specimen, to Figure 2 of the finite-element-model geometry, it can be seen that: (i) the actual gripping portion of the specimen is not modelled (however, the restraints are correctly represented), and (ii) actual bolts/holes are not included in the model. Model 1 incorporates rigid joints between the components. Model 2 and Model 3 use 'repeated freedoms' and 'gap elements', at the interface between components in an effort to model the bolts/holes, and hence, the bending behaviour of the bolted joint. Model 3 is similar to Model 2, the difference being the number of repeated-freedoms pairs and hence gap elements.

Repeated freedoms are employed to restrict linked nodes (pairs) to move identically, hence, they always remain a fixed distance apart (0.001 mm, for Models 2 and 3). They model the areas of the specimens where the components are, effectively, connected by the compressive stresses produced by the torqued bolts. Gap elements are also used to restrict the movement of linked nodes, however, in a limited way. They enable the adjacent components to separate and slide but not to overlap, and thus, model the areas of the specimen adjacent to the bolts, which are out of the influence of the compressive stresses of the bolts.

The increase in *width* of the ends of the specimen is accounted for in the two-dimensional models by a change in *depth* of the relevant elements. The increase in width of the

extensions is modelled by three rectangles; the total area of the extensions of the model being equivalent to that of the extensions of the specimen. The elements of the controlling and test sections have a depth of 51 mm. The depth of the elements at the thinnest end of the extension is 51.5 mm for a length of 26 mm, the depth then increases to 59.5 mm for 13 mm, and lastly, to 72 mm for 13 mm at the end of the extension; the total length of each extension is equal to the sum of 26, 13 and 13 (52 mm). The local neutral axis (y-direction) positions relative to that for the applied load are: -1.0 mm for the left-hand extension, +1.5 mm for the test section, 0 mm for the controlling section, and +0.625 mm for the right-hand extension.

In all three models a uniform tensile stress is applied to the right-hand end of the model. The left-hand end is restrained from moving horizontally and vertically, and all end nodes are restricted to moving horizontally together (Figure 2(a)). These restraints model the specimen as if it is gripped in a fatigue test machine. The resultant finite element mesh (Figure 2(b)) consists of 582 eight-noded isoparametric quadrilateral elements. Model 1 has 1957 nodes and Models 2 and 3 have 2035 nodes. Listings of the finite element data files for Model 1 and Model 3 are given in Appendices A and B, respectively. To enable comparison between the theoretical and experimental stress distribution data, the bulk-stress ( $\sigma_x + \sigma_y$ ) contour plots for each of the models, under an applied tensile stress of 16.4 MPa are given in Figures 3(a)-(c). The stress value of 16.4 MPa is equivalent to the maximum tensile stress applied to the experimental specimen. Figure 4 is the displacement diagram obtained from Model 3.

The PAFEC (Program for Automatic Finite Element Calculations) suite of programs was used on an 'Apollo DN10000' machine with the 'Apollo Domain/OS Version SR10.3' operating system for this work.

### 3.1 Model 1

Model 1 has 'welded' joints. The joints between the three components are rigid, i.e., the specimen is modelled as a single machined article.

### 3.2 Model 2

Model 2 uses repeated freedoms and gap elements to join the three separate components. A gap of 0.001 mm between the components is introduced. The repeated freedoms join pairs of nodes on adjacent components at the bolt sites and extend either side of the 'bolt' diameters to the next and following corner nodes (i.e., a further two elements on each side from the edges of the bolts). A total of forty-one (41) separate pairs of nodes are forced to move as single nodes by using repeated freedoms, joining the components together in three locations. This simulates the 'forcing together' of surfaces of the bolted joint of the specimen. Gap elements are used to link the components at all nodes either side of the 'bolts' (thirty-seven (37) separate pairs).

### 3.3 Model 3

Model 2 was found to be too rigid in the vicinity of the bolts, thus Model 3 employs less repeated freedoms and more gap elements than Model 2. The repeated freedoms in Model 3 are used at the bolt sites only. A total of seventeen (17) separate pairs of nodes are forced to move as single nodes using repeated freedoms, and sixty-one (61) separate pairs of nodes are linked by gap elements.

#### 4. EXPERIMENTAL ANALYSIS

SPATE (Stress Pattern Analysis by measurement of Thermal Emission) testing was performed on a secondary-bending specimen which had cold-expanded bolt holes and interference-fit bolts (specimen SQ75). The SPATE 8000 system used in this experimental analysis, detects emitted thermal energy from a specimen under cyclic stress. It scans a preselected area and an uncalibrated stress contour plot of  $(\sigma_x + \sigma_y)$  is obtained point by point.

A constant alternating load of 0.5 – 10.5 kN (0.78 – 16.4 MPa) was applied and the following scans taken, with 'front', 'back', 'right' and 'upper' orientations as per Figure 1:

- 1 Right side scan, from front angle of 15° off axis, with SPATE detector-head 56 cm from specimen (resolution 5),
- 2 Right side scan, from rearward angle of 15° off axis, with SPATE detector-head 66 cm from specimen (resolution 5),
- 3 Front scan of upper bolts, with SPATE detector-head 31 cm from specimen (resolution 4), and
- 4 Back scan of upper bolts, with SPATE detector-head 41 cm from specimen (resolution 4).

Scans 1 and 2 can be compared with finite element results once the corresponding area is outlined (Figures 5, 6 and 3). Scans 3 and 4 (Figures 7 and 8) highlight the three-dimensional nature of the stress distribution in the specimen.

#### 5. DISCUSSION OF RESULTS

A sketch of the joint section of the specimen is incorporated for clarity in Figure 5 (scan 1) and Figure 6 (scan 2). Figure 3(d) is a side view only of Figure 5 which enables comparison between the numerical stress contour plots of Figures 3(a)-(c) and the experimental data. Information regarding the secondary-bending ratio [3] is included in Appendix C.

##### 5.1 Numerical Analysis

In comparing the bulk-stress  $(\sigma_x + \sigma_y)$  contour plots of Model 1, Model 2 and Model 3 (in Figures 3(a)-(c)), it can be seen in all three that the:

- (i) stress flows through each component,
- (ii) main component carries the highest average stress,
- (iii) stress decreases as  $y$  decreases in the extension of the main component,
- (iv) stress decreases as  $y$  decreases and then changes such that stress increases as  $y$  decreases in the test section of the main component,
- (v) stress increases as  $y$  decreases in the extensions of the secondary components, and
- (vi) 'free ends' of the components carry a very low (or negative) stress.

Figure 3(a) also highlights the sharp-edge stress raisers. Figures 3(b) and 3(c) show the singularities caused by a change in stiffness at the interface of the repeated freedoms and gap elements. They also indicate that the 5 mm thick secondary component carries the least stress.

The displacement diagram of Figure 4 confirms the occurrence of points (iii), (iv) and (v) above, i.e., bending. The models bend similarly to Figure 4 due to the neutral axis of; the left-hand extension being lower by 1.0 mm, the test section being higher by 1.5 mm, and the

right-hand extension being higher by 0.625 mm, than that of the rest of the model. When the specimen experiences an applied tensile stress, these three areas, due to end constraints, try to align their neutral axes with that of the gripped sections (located at  $y = -6.5$  mm).

## 5.2 Experimental Analysis

Figures 5 and 6 are SPATE scans 1 and 2 respectively, with an over-sketch of the specimen for clarity. The presence of the SPATE signal outside the boundary of the specimen is due to limitations in the depth of field of the infrared detector. These two figures clearly show:

- (i) the stress distribution through components,
- (ii) that the main component experiences the highest average stress,
- (iii) that the main component carries a high stress in the front face under the upper set of bolts,
- (iv) that the thin secondary component takes the next highest average stress,
- (v) that the thick secondary component experiences the lowest average stress,
- (vi) the stress gradient across the thickness of each component, and
- (vii) that the 'free ends' of the components carry minimal stress.

Figures 7 and 8 indicate the following, where the 'upper' and 'lower' set of bolts are as shown in Figure 1:

- (i) the three-dimensional nature of the stress field in the vicinity of the bolt holes,
- (ii) that the main component carries a maximum stress under the upper set of bolts,
- (iii) that the thin component experiences minimal stress above the lower set of bolts,
- (iv) that the main component carries a greater stress on its back (compared to its front), and
- (v) that the thick secondary component experiences a small amount of stress immediately under the upper set of bolts.

Therefore, the SPATE scans provide information regarding the stress distribution, including the bending characteristics of the specimen.

## 5.3 Comparison of Experimental and Numerical Analyses

The general trend of the specimen's load-transfer characteristics can be obtained from the finite element models as seen in Section 5.1. The bending behaviour of the experimental specimen is also consistent with the displacement diagram of Model 3 (Figure 4).

However, local values gained from the numerical analysis do not correlate well with the experimentally acquired data at certain regions, Figure 9 (and Appendix C). The capability of the finite element models to represent an actual specimen is summarised in Figure 9. Average values of bulk stress were obtained at the five designated points (A, B, C, D, and E) from each of the three finite element models and from the SPATE scan number 1. Using the axis system of Figure 2(a), the coordinates of the five locations are as follows:

Point coordinates

Point	X	Y
A	-13.0	-7.5
B	2.9	-2.5
C	57.5	-2.5
D	44.0	-7.5
E	57.5	-11.5

Points A to E are located in the centre of the thickness of the components, and the bulk-stress value of each point was determined by taking the average of it plus its four adjacent data points, where the data points, for the numerical models, are elements, and for the experimental analysis, are SPATE measuring points. For each case (three numerical and one experimental), the value of bulk stress at points B, C, D, and E, were compared to the value at A. The relative bulk stress at points B and C show compliance for all cases, however, the stresses of the numerical models differ from the experimental data at point E, and especially at point D. Model 1, the 'welded joint' model, has relative bulk-stress values at points D and E which have much higher values than those for SPATE, indicating that a much greater relative stress is experienced by the 'free ends' of the components. Models 2 and 3 show the reverse; the 'free ends' sustain negligible or negative stress compared to SPATE. Therefore, a three-dimensional numerical model which displays characteristics between those of Model 1, and Models 2 and 3, is desired.

As expected, the differing finite element approaches bounded the true solution. It is believed that a three-dimensional model is necessary to obtain good agreement between numerical and experimental results at any location.

#### 5.4 Comparison of U.K. and Numerical Data

Experimental secondary-bending ratio data of similar specimens from the U.K. [2] were examined. Values of secondary-bending ratio were calculated from the finite element models and compared to the experimental information from the U.K. specimens (for more detail refer to Appendix C). The secondary-bending ratio is defined as 'the ratio of the bending strain and the axial strain at the position under consideration' [3], and the values from the various models, at a stress equal to that used for the SPATE measurements, are as follows;

Secondary-bending ratio at an applied stress of 16.4 MPa

Model No.	Secondary-bending ratio
1	-0.3616
2	-0.2186
3	0.5446

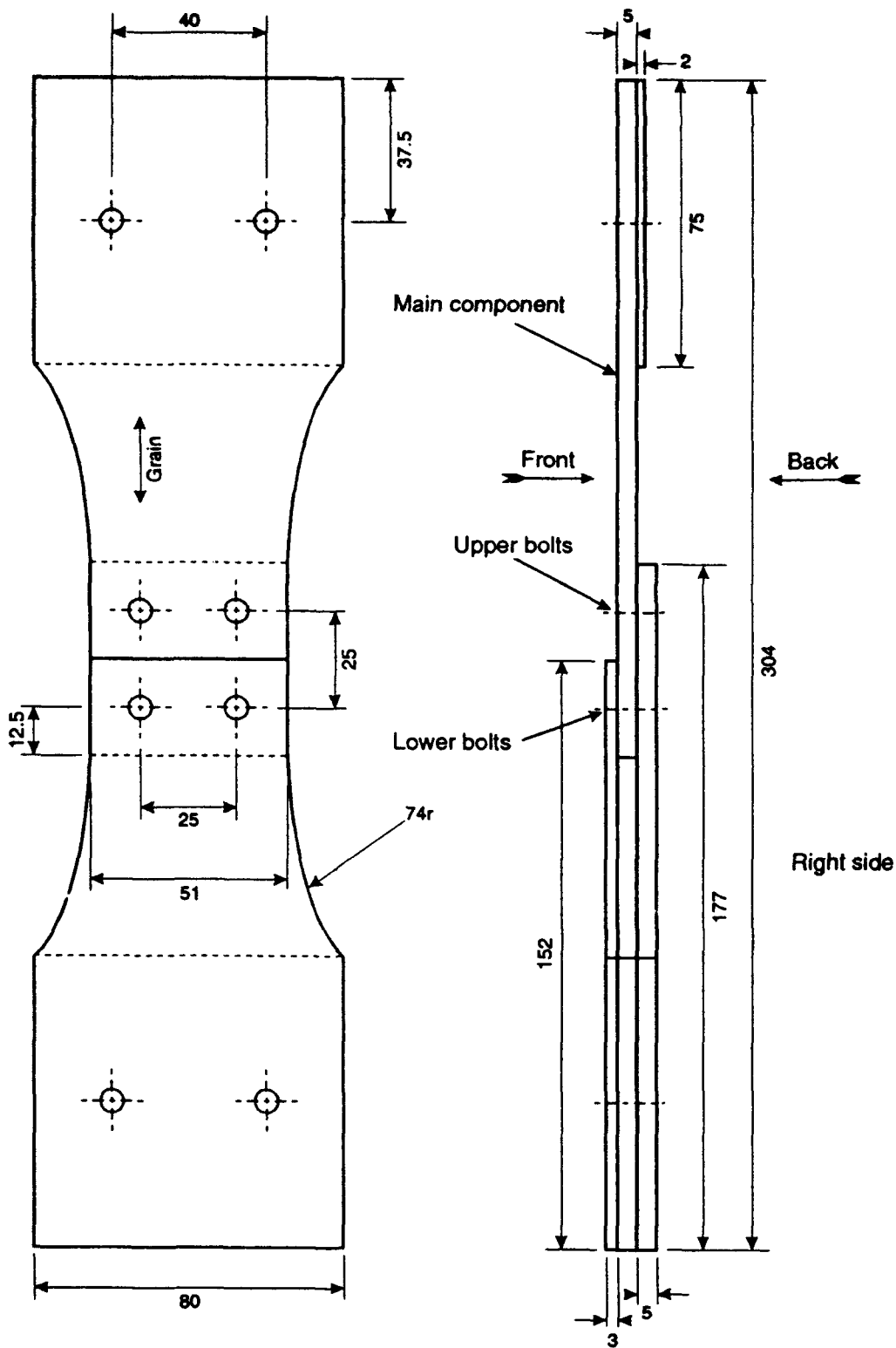
Model 3 predicts the correct sign of the secondary-bending ratio, however, the values of secondary-bending ratio for Model 3 are unduly increased by stress concentrations at the nearby repeated-freedom/gap-element interface. The values of secondary-bending ratio for all three numerical models remain virtually constant with change in applied stress, in contrast to the experimental data, where the values of secondary-bending ratio increase with increase in stress. The experimental U.K. values of secondary-bending ratio range from 0.13 at an applied stress of 17 MPa, to 0.494 at the maximum applied stress of 104.7 MPa. As mentioned above, it is believed that a three-dimensional model is necessary to obtain good agreement between numerical and experimental results at specific locations.

## 6. CONCLUSIONS

1. This Note has shown that the general trends of the load-transfer characteristics of the secondary-bending specimen can be obtained from two-dimensional finite element models.
2. Stresses from specific regions of a two-dimensional finite element model do not satisfactorily compare to the behaviour of an actual secondary-bending bolted joint specimen. Difficulty was experienced in obtaining the correct load transfer through the bolts. Model 1 resulted in too much load transfer and Models 2 and 3 in too little. A theoretical model which gives results between a welded model and one using repeated freedoms and gap elements is desired.
3. The values of secondary-bending ratio for the two-dimensional models did not agree with those obtained experimentally (from the U.K.). Of the three models, Model 3 gave the most reasonable results. The experimental values of secondary-bending ratio were calculated using strain-gauge data. The location of these strain gauges was very close to the bolt holes. Clearly, three-dimensional effects dominate in the region of bolt holes, thus, a two-dimensional model is inadequate. It is believed that a three-dimensional model to represent the secondary-bending specimen is essential for the generation of more consistent results.

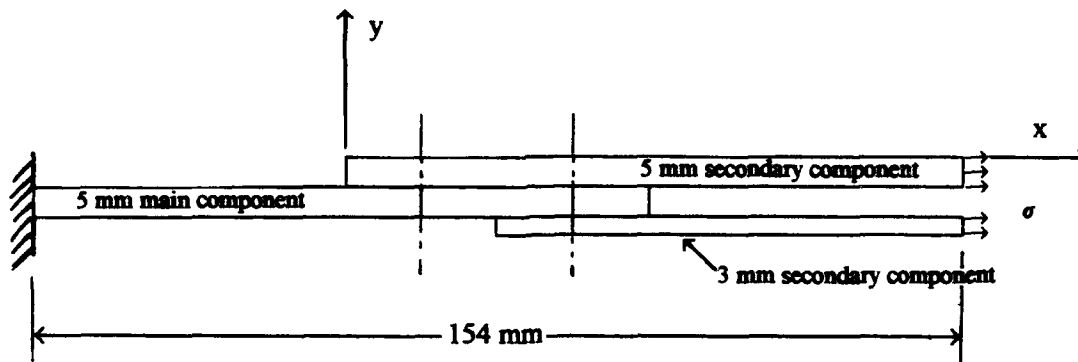
## REFERENCES

1. RL Evans, "The Influence of Secondary Bending on Fatigue Life Improvement in Bolted Joints", Aug 1993. ARL-RR-14.
2. R Cook, "Standard Fatigue Test Specimens for Fastener Evaluation", Nov 1987. AGARD-AG-304.
3. HH van der Linden (Ed.), "Fatigue Rated Fastener Systems - An AGARD Coordinated Testing Program", May 1985. AGARD-R-721.

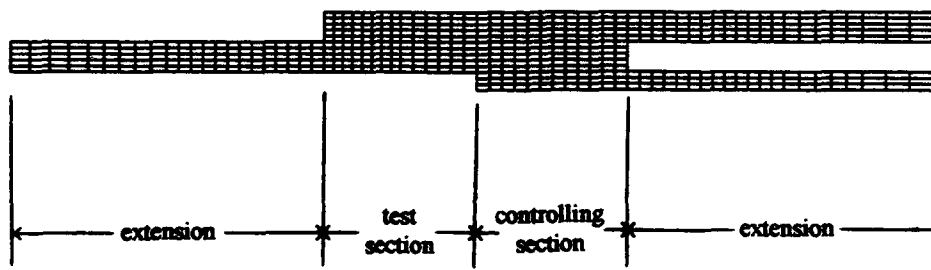


Dimensions in mm

FIGURE 1: ARL Secondary-bending specimen



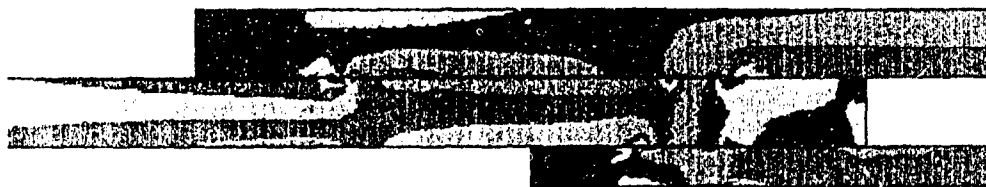
(a): Finite element model of the ARL secondary-bending specimen



(b): Finite element mesh of the ARL secondary-bending specimen

FIGURE 2: Two-dimensional finite element model

-23.1      10.7      44.5      78.4    MPa



(c): Contour plot of bulk stress ( $\sigma_x + \sigma_y$ ) for Model 3, with applied stress of 16.4 MPa

0                      300    units



(d): SPATE scan number 1 at an applied stress of 16.4 MPa

FIGURE 3: Comparison of numerical and experimental bulk-stress distributions



FIGURE 4: Displacement diagram from Model 3 under a tensile stress

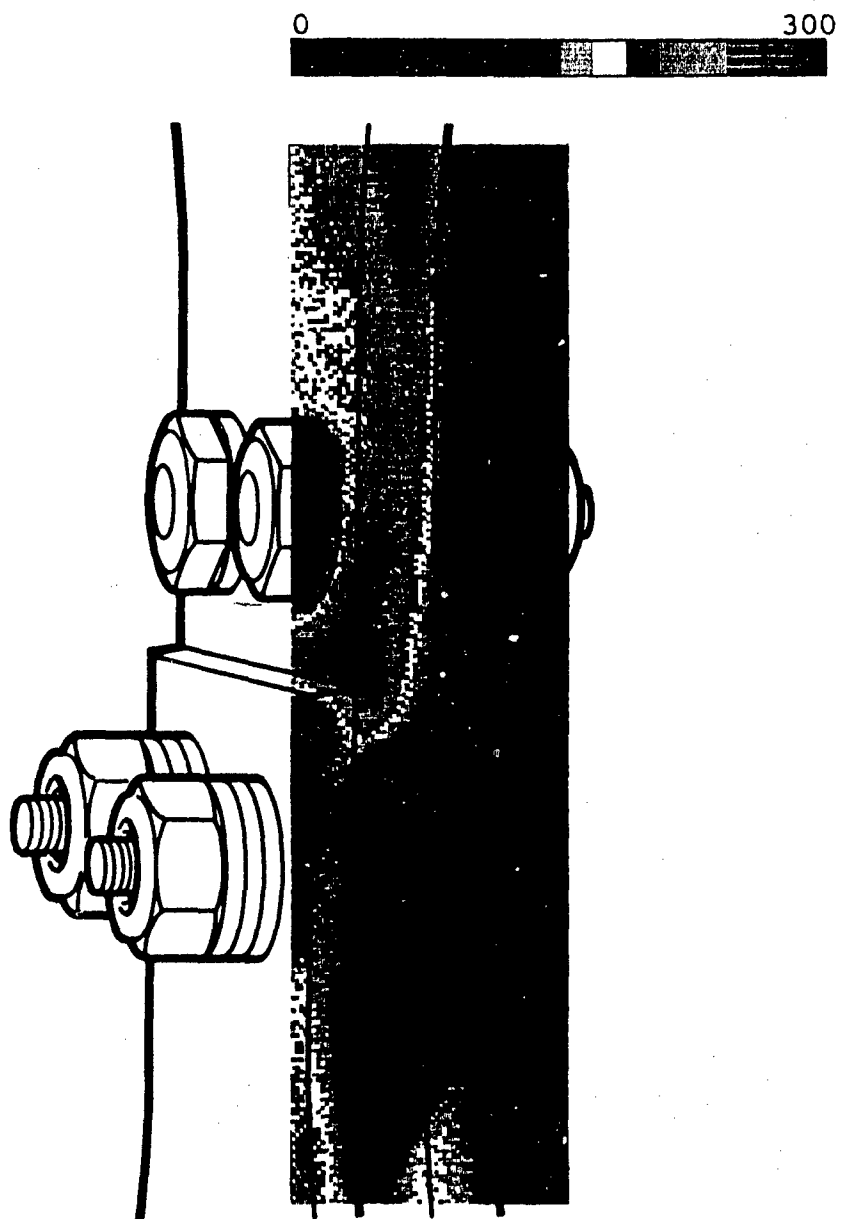


FIGURE 5: Right side SPATE scan from front angle (scan 1)

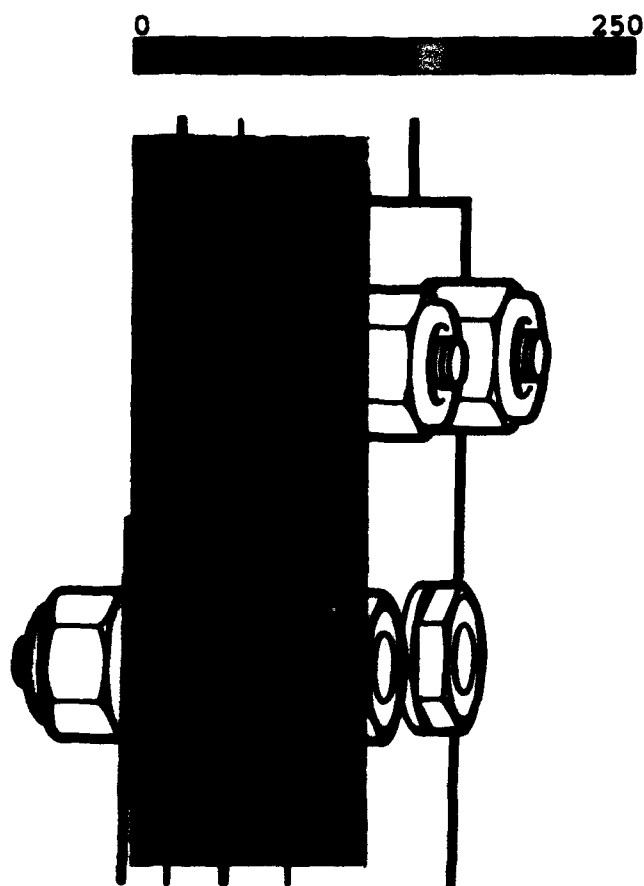


FIGURE 6: Right side SPATE scan from back angle (scan 2)



FIGURE 7: SPATE scan of front of specimen (scan 3)

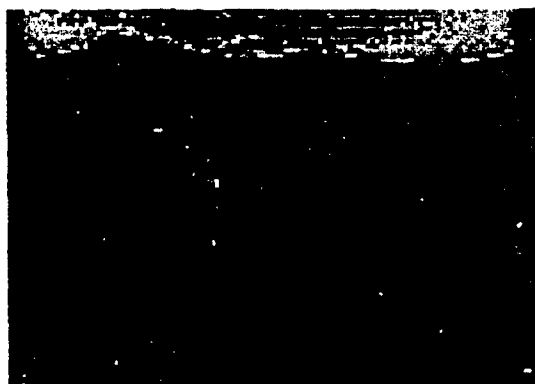


FIGURE 8: SPATE scan of back of specimen (scan 4)

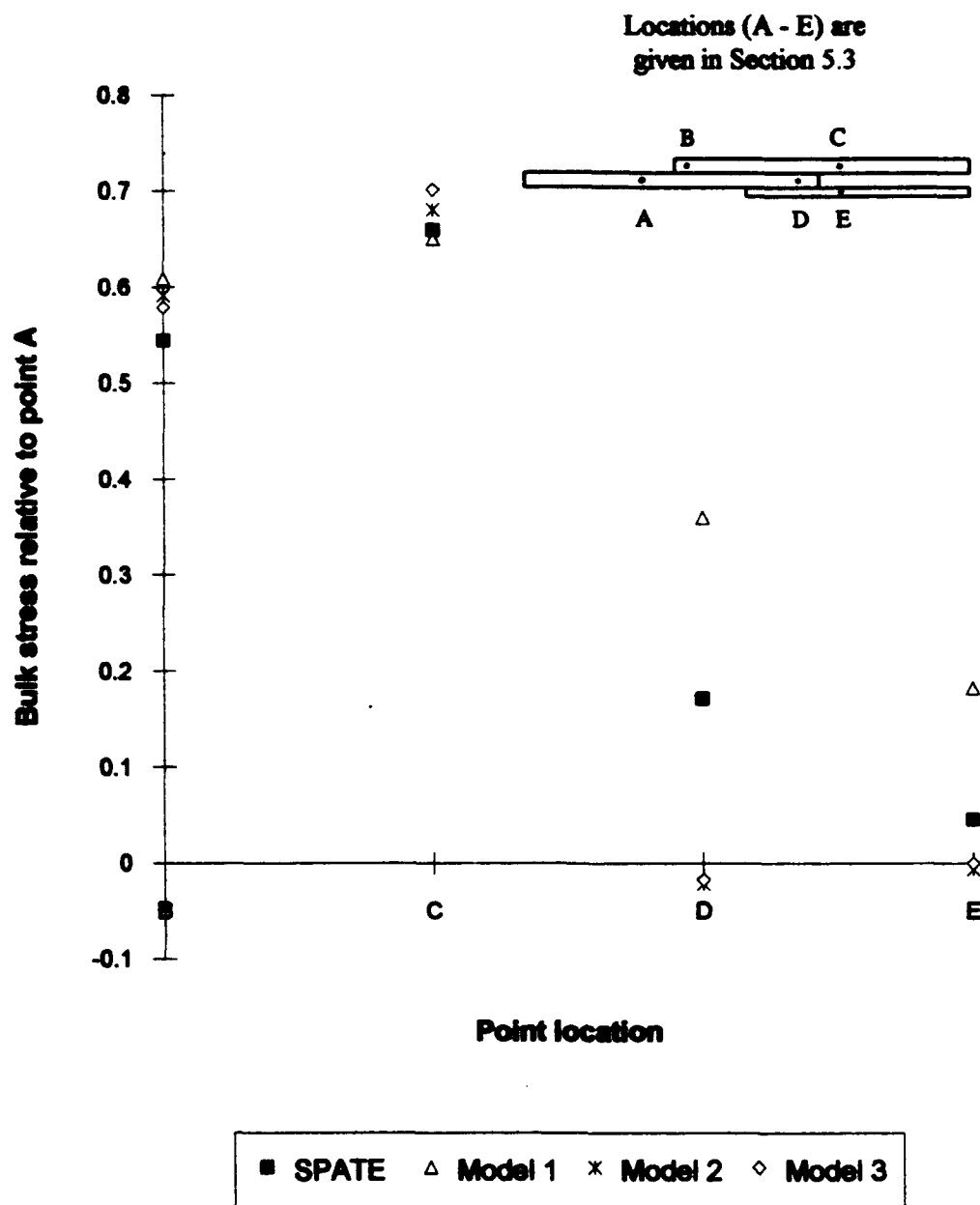


FIGURE 9: Ratio of point bulk stresses relative to values at point A

## APPENDIX A: PAFEC data file for Model 1

C DATA FOR THE 2D ANALYSIS OF A SECONDARY BENDING SPECIMEN.  
C  
C THE SECONDARY BENDING SPECIMEN IS MODELLED AS A SOLID COMPONENT  
C - A 'WELDED' JOINT. THE LHS IS FIXED, THE RHS IS RESTRAINED IN  
C THE VERTICAL PLANE ONLY AND THE LOAD APPLIED IN THE HORIZONTAL  
C PLANE. THE 'WAISTING' OF THE SPECIMEN IS MODELLED IN THREE  
C RECTANGULAR STEPS. NOTE: Y (DATA FILE) = -Y (FIGURES IN REPORT)

C  
CONTROL  
FULL.CONTROL  
TOLERANCE=1E-4  
PHASE=1  
PHASE=2  
PHASE=4  
PHASE=6  
PHASE=7  
PHASE=9  
USE.STREN  
CONTROL.END

C NODES NODE . NUMBER	X	Y
1	0	0
2	12.5	0
3	25.0	0
4	37.5	0
5	50.0	0
6	102.0	0
7	-52.0	5.0
8	0	10.0
9	12.5	15.0
10	25.0	20.0
11	37.5	25.0
12	50.0	30.0
13	102.0	35.0
14	-52.0	40.0
15	0	45.0
16	12.5	50.0
17	25.0	55.0
18	37.5	60.0
19	50.0	65.0
20	102.0	70.0
21	25.0	13.0
22	37.5	18.0
23	50.0	23.0
24	102.0	28.0
C		
25	76.0	0
26	89.0	0
27	-39.0	5.0
28	-26.0	10.0
29	76.0	5.0
30	89.0	10.0
31	-39.0	15.0
32	-26.0	20.0
33	76.0	10.0
34	89.0	15.0
35	76.0	13.0
36	89.0	18.0

```

C
PAFBLOCKS
ELEMENT TYPE=36210
PROPERTIES=11
BLOCK. GROUP. N1 N2 TOPOLOGY
1 1 1 7 1 2 8 9
2 2 2 7 2 3 9 10
3 3 3 7 3 4 10 11
4 4 4 7 4 5 11 12
7 5 1 8 8 9 15 16
8 6 2 8 8 10 16 17
9 9 3 8 10 11 17 18
10 10 4 8 11 12 18 19
11 11 3 9 17 18 21 22
12 12 4 9 18 19 22 23

```

```

C
PAFBLOCKS
ELEMENT.TYPE=36210
PROPERTIES=12
BLOCK.  GROUP.  N1      N2      TOPOLOGY
14      14      10      7      5,25,12,29
15      15      10      8      28,8,32,15
16      16      10      9      19,33,23,35

```

```

C
PAFBLOCKS
ELEMENT.TYPE=36210
PROPERTIES=13
BLOCK.  GROUP.  N1      N2      TOPOLOGY
17      17      11      7      25, 26, 29, 30
18      18      11      8      27, 28, 31, 32
19      19      11      9      33, 34, 35, 36

```

```

C
PAFBLOCKS
ELEMENT.TYPE=36210
PROPERTIES=14
BLOCK.  GROUP.  N1      N2      TOPOLOGY
20      20      12      7      26,6,30,13
21      21      13      8      7,27,14,31
22      22      12      9      34,20,36,24

```

C	END OF PAFBLOCKS
C	
C	
MESH	
REFERENCE	SPACING.LIST
1	8
2	6
3	6
4	6
7	5
8	5
9	3

```

C
10
11      13
12      5
13      4, 4, 4, 1
14      4
C
END OF MESH
C
MATERIAL
MATERIAL.NUMBER      E      NU
11      71000      0.33
C
END OF MATERIAL
C
PLATES.AND.SHELLS
PLATE      MATERIAL.NUMBER      THICKNESS
11      11      51
12      11      51.5
13      11      59.5
14      11      72
C
END OF PLATES.AND.SHELLS
C
RESTRAINTS
NODE.NUMBER      PLANE      DIRECTION
7      1      12
1789      1      2
C
REPEATED.FREEDOMS
N1 N2      PLANE      DIRECTION
6 0      1      1
C
END OF RESTRAINTS
C
SURFACE.FOR.PRESSURE
PRESSURE.VALUE      NODE      PLANE
-16.4      6      1
C
END OF PRESSURE
C
END.OF.DATA

```

## APPENDIX B: PAFEC data file for Model 3

```

C DATA FOR THE 2D ANALYSIS OF A SECONDARY BENDING SPECIMEN
C THIS SECONDARY BENDING SPECIMEN IS MODELLED AS THREE SEPARATE COMPONENTS
C USING REPEATED FREEDOMS AND GAP ELEMENTS. THE TEST MACHINE GRIP SECTIONS
C ARE NOT MODELLED. THE REPEATED FREEDOMS ARE APPLIED AT THE BOLT SITES
C ONLY. THE LHS IS FIXED, THE RHS IS RESTRAINED IN THE VERTICAL PLANE ONLY
C AND THE LOAD APPLIED IN THE HORIZONTAL PLANE. THE 'WAISTING' OF THE
C SPECIMEN IS MODELLED IN THREE RECTANGULAR STEPS.
C NOTE: Y (DATA FILE) = -Y (FIGURES IN REPORT)
C
C CONTROL
C FULL CONTROL
C TOLERANCE=1E-4
C PHASE=1
C PHASE=2
C PHASE=4
C PHASE=6
C PHASE=7
C GAP ITERATION=20
C PHASE=9
C USE STREN
C CONTROL END
C
C NODES
C NODE NUMBER
C
C 1 0 0
C 2 12.5 0
C 3 25.0 0
C 4 37.5 0
C 5 50.0 0
C 6 102.0 0
C 7 0 4.999
C 8 12.5 4.999
C 9 25.0 4.999
C 10 37.5 4.999
C 11 50.0 4.999
C 12 102.0 4.999
C 13 0 5.0
C 14 12.5 5.0
C 15 25.0 5.0
C 16 37.5 5.0
C 17 50.0 5.0
C 18 102.0 5.0
C 19 0 9.999
C 20 12.5 9.999
C 21 25.0 9.999
C 22 37.5 9.999
C 23 50.0 9.999
C 24 102.0 9.999
C 25 0 10.0
C 26 12.5 10.0
C 27 25.0 10.0
C 28 37.5 10.0
C 29 50.0 10.0
C 30 102.0 10.0
C 31 0 13.0
C 32 12.5 13.0
C 33 25.0 13.0
C 34 37.5 13.0
C 35 50.0 13.0
C 36 102.0 13.0
C 37 76.0 0.0
C 38 89.0 0.0
C 39 -39.0 5.0
C 40 -26.0 5.0
C 41 76.0 4.999
C 42 89.0 4.999
C 43 -39.0 9.999
C 44 -26.0 9.999
C 45 76.0 10.0
C 46 89.0 10.0
C 47 76.0 13.0
C 48 89.0 13.0
C
C PAFBLOCKS
C ELEMENT TYPE=36210
C PROPERTIES=11
C BLOCK. GROUP. N1 N2 TOPOLOGY
C 1 1 1 7 1,2,7,8
C 2 2 2 7 2,3,8,9
C 3 3 3 7 3,4,9,10
C 4 4 4 7 4,5,10,11
C 7 7 1 8 14,15,20,21
C 8 8 2 8 15,16,21,22
C 9 9 3 8 16,17,22,23
C 10 10 4 8 17,18,23,24
C 11 11 3 9 25,26,29,30
C 12 12 4 9 26,27,30,31
C
C PAFBLOCKS
C ELEMENT TYPE=36210
C PROPERTIES=12
C BLOCK. GROUP. N1 N2 TOPOLOGY
C 14 14 10 7 5,33,11,37
C 15 15 10 8 36,14,40,20
C 16 16 10 9 27,41,31,43
C
C PAFBLOCKS
C ELEMENT TYPE=36210
C PROPERTIES=13
C BLOCK. GROUP. N1 N2 TOPOLOGY
C 17 17 11 7 33,34,37,38
C 18 18 11 8 35,36,39,40
C 19 19 11 9 41,42,43,44
C
C PAFBLOCKS
C ELEMENT TYPE=36210
C PROPERTIES=14
C BLOCK. GROUP. N1 N2 TOPOLOGY
C 20 20 12 7 34,6,38,12
C 21 21 13 8 13,35,19,39
C 22 22 12 9 42,28,44,32
C
C END OF PAFBLOCKS
C

```

```

MESH
REFERENCE          SPACING.LIST
1
2
3
4
7
8
9
C
10
11
12
13
C
C
C
END OF MESH
C
MATERIAL
MATERIAL.NUMBER    E          NU
11                  71000      0.33
C
C
END OF MATERIAL
C
PLATES.AND.SHELLS
PLATE              MATERIAL.NUMBER    THICKNESS
11                 11                 51
12                 11                 51.5
13                 11                 59.5
14                 11                 72
C
C
END OF PLATES.AND.SHELLS
C
RESTRAINTS
NODE.NUMBER        PLANE          DIRECTION
13                 1              12
1867               1              2
C
C
MODELLING OF BOLTS
C
REPEATED.FREEDOMS
N1 N2              PLANE          DIRECTION
6 0                 1              1
C
186 501            0              0
187 502            0              0
8 15               0              0
277 631            0              0
278 632            0              0
C
386 740            0              0
387 741            0              0
10 17              0              0
477 831            0              0
478 832            0              0
C
827 938            0              0
828 939            0              0
829 940            0              0
830 941            0              0
23 26              0              0
920 1000           0              0
921 1001           0              0
C
C
END OF RESTRAINTS
C
GAPS
DIRECTION=2
TYPE=1
OFFSET=0.001
N1 N2              NUMBER.OF.GAP
7 14               1
173 488            2
174 489            3
175 490            4
176 491            5
177 492            6
178 493            7
179 494            8
180 495            9
181 496            10
182 497            11
183 498            12
184 499            13
185 500            14
C
279 633            15
280 634            16
281 635            17
282 636            18
283 637            19
284 638            20
285 639            21
286 640            22
287 641            23
9 16               24
377 731            25
378 732            26
379 733            27
380 734            28
381 735            29
382 736            30
383 737            31
384 738            32
385 739            33
C
479 833            34
480 834            35
481 835            36
482 836            37
483 837            38
484 838            39
485 839            40
486 840            41
487 841            42
11 18              43

```

25	22	44
820	931	45
821	932	46
822	933	47
823	934	48
824	935	49
825	936	50
826	937	51
C		
922	1002	52
923	1003	53
924	1004	54
925	1005	55
926	1006	56
927	1007	57
928	1008	58
929	1009	59
930	1010	60
24	27	61

C  
 C SURFACE.FOR.PRESSURE  
 C PRESSURE.VALUE NODE PLANE  
 C -16.4 6 1  
 C  
 C END OF PRESSURE  
 C  
 C END.OF.DATA

## APPENDIX C: Secondary-bending ratio data

Experimental secondary-bending ratio (SBR) data of similar specimens from the United Kingdom [C1] were examined. Values of SBR were obtained from the finite element models and compared to the experimental information from the U.K. specimens.

From [C2], the SBR is defined as:

$$\begin{aligned} \text{SBR} &= \frac{\text{STRAIN}_{\text{BENDING}}}{\text{STRAIN}_{\text{AXIAL}}} \\ &= \frac{(\text{STRAIN}_2 - \text{STRAIN}_1) / 2}{(\text{STRAIN}_2 + \text{STRAIN}_1) / 2} \end{aligned}$$

Thus,

$$\text{SBR} = \frac{\text{STRESS}_2 - \text{STRESS}_1}{\text{STRESS}_2 + \text{STRESS}_1}$$

Reference C2 also indicates the position of the strain gauges for experimental calculation of the SBR. SBR values were determined for the three finite element models using the information from these references, where node positions 'X' in Figure C1 are equivalent to strain-gauge locations. Stress values in adjacent elements to nodes X were averaged for the SBR calculation. Obviously the full array of strain gauges could not be duplicated on a two-dimensional model. The profile of the specimen, and thus the profile of the strain-gauge locations, were represented.

The values of SBR for the three numerical models remain virtually constant with change in applied stress (Table C1) in contrast to the experimental data of reference C1 (Table 8) where the values of SBR increase with increase in stress. The experimental U.K. values of SBR range from 0.13, 0.22 (loading, unloading) at an applied stress of 17 MPa, to 0.48, 0.42 at an applied stress of 52 MPa, to 0.494 at the maximum applied stress of 104.7 MPa. An applied stress of 104.7 MPa is equivalent to a net-area stress of 350 MPa in the test section of the main component. Model 1 and Model 2 have rigid connections (repeated freedoms) at the location of the nodes used in the SBR calculation which results in the negative values of SBR, i.e., the value of  $\sigma_{x(2)}$  is unrealistically reduced due to the excessive restraints. The nodal stress values ( $\sigma_{x(1)}$  and  $\sigma_{x(2)}$ ) increase with increase in applied stress, however, they do so in the same ratio, resulting in the same SBR. The use of gap elements (as compared to repeated freedoms) at the significant locations of Model 3, improves the SBR values, i.e., they are positive. Model 3 predicts the correct sign of SBR. However, stress concentrations at the repeated-freedom/gap-element interface unduly increase the value of  $\sigma_{x(2)}$ , thus, the SBR.

The SBR was determined at locations either side of the strain gauges for the three models (refer to Table C2 and Figure C1) to investigate the sensitivity of SBR with position. The relatively stiff Model 1 has a small difference in SBR values, whereas Models 2 and 3 display a wide range in values, over the seven positions, i.e., the SBR calculations of the less rigid models are more sensitive to location. The SBR at position 1 for Model 2 could not be calculated as the stress values in the adjacent elements were too extreme. This is due to position 1 being the location of a repeated-freedom/gap-element interface for this model.

The discrepancies between the experimental and theoretical SBR values are not unexpected. The location of the strain gauges are tangential to the bolt-hole edges, hence three-dimensional effects are very important. Around the region of the holes, the two-dimensional finite element models inadequately represent the strain-gauge values of the actual secondary-bending specimen.

## References

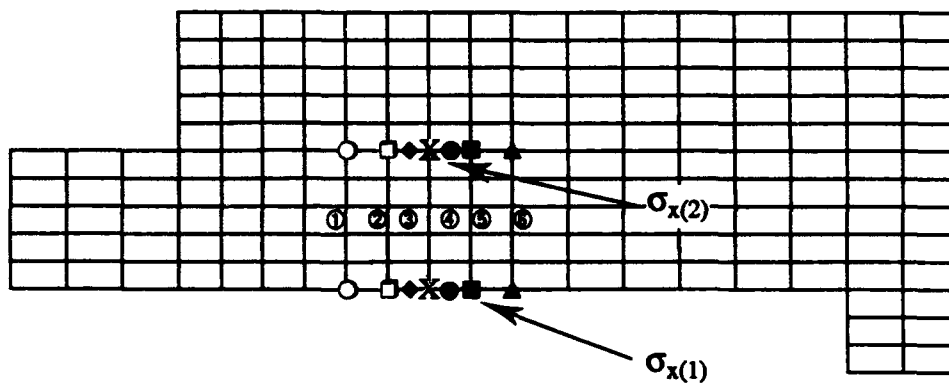
- C1. R Cook, "Standard Fatigue Test Specimens for Fastener Evaluation", Nov 1987. AGARD-AG-304.
- C2. HH van der Linden (Ed.), "Fatigue Rated Fastener Systems - An AGARD Coordinated Testing Program", May 1985. AGARD-R-721.

**TABLE C1**  
Secondary-bending ratio versus applied stress  
for Model 1, Model 2, and Model 3

Model No.	Applied stress (MPa)	Average stress <sub>x(1)</sub> (MPa)	Average stress <sub>x(2)</sub> (MPa)	Secondary-bending ratio
1	4.1	9.937	4.659	-0.3616
	16.4	39.773	18.647	-0.3616
	104.7	253.736	118.960	-0.3616
2	4.1	8.541	5.482	-0.2181
	16.4	34.213	21.937	-0.2186
	104.7	218.369	139.929	-0.2189
3	4.1	4.383	15.006	0.5479
	16.4	17.660	59.898	0.5446
	104.7	114.011	380.458	0.5389

**TABLE C2**  
Variation in secondary-bending ratio for an applied stress of 104.7 MPa

Model No.	SBR calculation position						
	1	2	3	X	4	5	6
1	-0.3424	-0.3569	-0.3589	-0.3616	-0.3613	-0.3615	-0.3591
2	—	-0.0413	-0.1419	-0.2189	-0.2543	-0.2918	-0.3295
3	0.4999	0.5180	0.5150	0.5389	0.5924	0.4851	-0.0454



- X            representative location of the U.K. strain gauges
- , □, ◆,    location of pairs of stress values 1 to 6 respectively
- , ■, ▲

FIGURE C1: Location of stress<sub>x(1)</sub> and stress<sub>x(2)</sub> for the calculation of secondary-bending ratio

## **DISTRIBUTION**

### **AUSTRALIA**

#### **DEFENCE ORGANISATION**

##### **Defence Science and Technology Organisation**

Chief Defence Scientist  
FAS Science Policy  
AS Science Corporate Management } shared copy  
Counsellor Defence Science, London (Doc Data Sheet only)  
Counsellor Defence Science, Washington (Doc Data Sheet only)  
Senior Defence Scientific Adviser (Doc Data Sheet only)  
Scientific Advisor Policy and Command (Doc Data Sheet only)  
Navy Scientific Adviser (3 copies Doc Data Sheet only)  
Scientific Adviser - Army (Doc Data Sheet only)  
Air Force Scientific Adviser

##### **Aeronautical Research Laboratory**

Director  
Library  
Chief Airframes and Engines Division  
Authors: R.L. Evans  
M. Heller

S. Galea  
J.M. Finney  
D. Rees  
A.S. Machin  
G.S. Jost  
P. Piperias

Materials Research Laboratory  
Director/Library

Main Library - DSTO Salisbury

##### **Defence Central**

OIC TRS, Defence Central Library  
Document Exchange Centre, DSTIC (8 copies)  
Defence Intelligence Organisation  
Library, Defence Signals Directorate (Doc Data Sheet Only)

##### **HQ ADF**

Director General Force Development (Air)

##### **Air Force**

AIRREG4-LC (2 copies)  
PDR AF  
OIC ATF, ATS, RAAFSTT, WAGGA (2 copies)

**Army**

Engineering Development Establishment Library  
US Army Research, Development and Standardisation Group (3 copies)

**Navy**

Director Aircraft Engineering - Navy  
Director of Naval Architecture

**UNIVERSITIES AND COLLEGES**

Australian Defence Force Academy  
Library  
Head of Aerospace and Mechanical Engineering

Melbourne  
Engineering Library

Monash  
Hargrave Library  
Head Materials Engineering  
Prof R. Jones, Mechanical Engineering

Newcastle  
Professor R. Telfer, Institute of Aviation

Sydney  
Engineering Library  
Head School of Civil Engineering  
Head School of Mechanical & Mechatronic Engineering  
Head School of Aeronautical Engineering

NSW  
Head, Mechanical Engineering

Tasmania  
Engineering Library

Western Australia  
Head Mechanical Engineering

RMIT  
Library  
Mr M.L. Scott, Aerospace Engineering

**OTHER GOVERNMENT DEPARTMENTS AND AGENCIES**

Department of Transport & Communication, Library  
AGPS  
SEC of Vic., Herman Research Laboratory  
Australian Nuclear Science and Technology Organisation  
Civil Aviation Authority

**OTHER ORGANISATIONS**

NASA (Canberra)

ASTA Engineering, Document Control Office

Ansett Airlines of Australia, Library

Qantas Airways Limited

Hawker de Havilland Aust Pty Ltd, Victoria, Library

Hawker de Havilland Aust Pty Ltd, Bankstown, Library

BHP Melbourne Research Laboratories

**UNITED KINGDOM**

Defence Research Agency (Aerospace)

Farnborough, R. Cook Materials and Structures

**SPARES (4 COPIES)**

**TOTAL (70 COPIES)**

PAGE CLASSIFICATION  
UNCLASSIFIED

PRIVACY MARKING

## DOCUMENT CONTROL DATA

1a. AIR NUMBER AR-008-404	1b. ESTABLISHMENT NUMBER ARL-TN-58	2. DOCUMENT DATE NOVEMBER 1993	3. TASK NUMBER AIR 92/069
4. TITLE  STRESS ANALYSIS OF A SECONDARY-BENDING SPECIMEN		5. SECURITY CLASSIFICATION (PLACE APPROPRIATE CLASSIFICATION IN BOX(S) IE. SECRET (S), CONF. (C), RESTRICTED (R), LIMITED (L), UNCLASSIFIED (U)).	6. NO. PAGES  25
		<div style="display: flex; justify-content: space-around;"> <div style="border: 1px solid black; padding: 2px; text-align: center;">U</div> <div style="border: 1px solid black; padding: 2px; text-align: center;">U</div> <div style="border: 1px solid black; padding: 2px; text-align: center;">U</div> </div> <div style="display: flex; justify-content: space-around; font-size: small;"> <span>DOCUMENT</span> <span>TITLE</span> <span>ABSTRACT</span> </div>	7. NO. REFS.  3
8. AUTHOR(S) R.L. EVANS M. HELLER		9. DOWNGRADING/DELIMITING INSTRUCTIONS  Not applicable.	
10. CORPORATE AUTHOR AND ADDRESS  AERONAUTICAL RESEARCH LABORATORY  AIRFRAMES AND ENGINES DIVISION  506 LORIMER STREET  FISHERMENS BEND VIC 3207		11. OFFICE/POSITION RESPONSIBLE FOR:  SPONSOR <u>RAAF AIRREG4-LC</u>  SECURITY <u>-</u>  DOWNGRADING <u>-</u>  APPROVAL <u>CAED</u>	
12. SECONDARY DISTRIBUTION (OF THIS DOCUMENT)  Approved for public release.  <small>OVERSEAS ENQUIRIES OUTSIDE STATED LIMITATIONS SHOULD BE REFERRED THROUGH DSTIC, ADMINISTRATIVE SERVICES BRANCH, DEPARTMENT OF DEFENCE, ANZAC PARK WEST OFFICES, ACT 2601</small>			
13a. THIS DOCUMENT MAY BE ANNOUNCED IN CATALOGUES AND AWARENESS SERVICES AVAILABLE TO ....  No limitations.			
13b. CITATION FOR OTHER PURPOSES (IE. CASUAL ANNOUNCEMENT) MAY BE			
<input checked="checked" type="checkbox"/> UNRESTRICTED OR		<input type="checkbox"/> AS FOR 13a.	
14. DESCRIPTORS Fatigue tests Two dimensional Finite element analysis Stress measurements			15. DISCAT SUBJECT CATEGORIES 201101 1305
16. ABSTRACT  <i>This Note describes a two-dimensional finite-element elastic analysis of a uniaxially-loaded bolted secondary-bending specimen which was conducted to provide information relevant to a recent ARL fatigue testing program. Three different approaches were employed to model the bolt/plate interface and the results are compared with thermoelastic stress measurements.</i>			

PAGE CLASSIFICATION  
**UNCLASSIFIED**

PRIVACY MARKING

THIS PAGE IS TO BE USED TO RECORD INFORMATION WHICH IS REQUIRED BY THE ESTABLISHMENT FOR ITS OWN USE BUT WHICH WILL NOT BE ADDED TO THE DATA DATA UNLESS SPECIFICALLY REQUESTED.

16. ABSTRACT (CONT).

17. IMPRINT

**AERONAUTICAL RESEARCH LABORATORY, MELBOURNE**

18. DOCUMENT SERIES AND NUMBER

Technical Note 58

19. WA NUMBER

21 227C

20. TYPE OF REPORT AND PERIOD COVERED

21. COMPUTER PROGRAMS USED

22. ESTABLISHMENT FILE REF.(S)

23. ADDITIONAL INFORMATION (AS REQUIRED)